*J. Fluid Mech.* (2006), *vol.* 552, *pp.* 419–440. © 2006 Cambridge University Press 
doi:10.1017/S0022112006008779 Printed in the United Kingdom

# Experiments at a two-scale dynamo test facility

By U. MÜLLER[1], R. STIEGLITZ[1] AND S. HORANYI[2]

[1]Forschungszentrum Karlsruhe GmbH, Postfach 3640, Universität Karlsruhe, 76021 karlsruhe, Germany

[2]Atomic Energy Research Institute, Budapest

(Received 26 October 2004 and in revised form 1 November 2005)

A report of experimental results on dynamo action is presented, obtained at the Karlsruhe dynamo test facility. Former observations concerning the properties of the dynamo magnetic field are corroborated and complemented. The feedback of the dynamo magnetic field on the sodium velocity in the test module is analysed based on measurements employing permanent magnet potential sensors. The evaluation of time signals recorded by these probes shows that a growing dynamo magnetic field transforms hydrodynamic turbulent velocity profiles in channels into magnetohydrodynamic slug flow profiles, indicating a balance between pressure and Lorentz forces. Cross-correlations between time signals of the magnetic induction and the local velocity reveal a significant coherency between apparently random fluctuations of these relevant dynamo quantities.

## 1. Introduction

It is generally accepted today that planetary and stellar magnetic fields originate from dynamo action in homogeneous, electrically conducting and circulating fluids in the interior of celestial bodies. This idea was first conjectured by Larmor (1919) and has been corroborated repeatedly by several geo- and astrophysicists who developed analytical and numerical models for this magnetohydrodynamic (MHD) process. Spectacular numerical calculations simulate even sophisticated geo- and astrophysical phenomena such as reversals of the geomagnetic field and the magnetodynamics of solar flairs. The progress in the development of dynamo modelling has been repeatedly summarized in survey articles, e.g. by Rädler (1999), Busse (2000), Glatzmaier & Roberts (2002) and in a textbook by Rüdiger & Hollerbach (2004). There has always been the desire to confirm the models for homogeneous dynamo action in laboratory experiment, but such experiments require equipment of dimensions that commonly exceed the capability of University Laboratories and may even challenge the technologies of major research establishments. Stieglitz & Müller (1996) and Cardin *et al.* (2002) have outlined this in some detail.

Lowes & Wilkinson (1968) first demonstrated experimentally the feasibility of homogeneous dynamos in electrically conducting continua. They avoided the problem of large devices by using ferromagnetic material and employing rigid-body rotation of solid steel cylinders in steel blocks (lubricated by liquid mercury at contacting boundaries). They followed a model conception of Herzenberg (1958) to achieve self-excitation of dynamo action. The design of an experimental hydromagnetic screw dynamo was pursued by Gailitis *et al.* (1989) in Riga, taking up an idea of Ponomarenko (1973). They showed successfully (Gailitis *et al.* 2000, 2001) that dynamo magnetic fields could be generated by helical sodium flow in coaxial pipes.

https://doi.org/10.1017/S0022112006008779 Published online by Cambridge University Press

A next step towards more generic flow topologies regarding geophysical application was made in the Karlsruhe dynamo experiment (Müller & Stieglitz 2000; Stieglitz & Müller 2001; Müller, Stieglitz & Horanyi 2004). Here, according to a proposal by Busse (1992), an arrangement of counter-rotating columnar vortices was realized by forced flow in a system of helical guide tubes placed in a container filled with sodium. In several test campaigns, a permanent dynamo magnetic field of dipole character was observed at this test facility and was analysed in some detail (Müller *et al.* 2004). The successful dynamo experiments in Riga and Karlsruhe have stimulated the efforts of other groups to plan and design magnetohydrodynamic dynamo experiments simulating the fluid flow topologies in planetary cores and stellar interiors more realistically. In particular, the large-scale feedback of the dynamo magnetic field on a free bulk flow pattern in planetary cores is the focus of such experiments. A survey of the respective experimental activities is given in Chossat, Armbruster & Oprea (2001), Gailitis *et al.* (2002) and Rädler & Cebers (2002). This target is beyond the capability of channelled sodium flows, as realized in the Riga and Karlsruhe test facilities.

Nevertheless, even if of limited use for geo- and astrophysical application, we considered an experimental investigation of the back-reaction of a growing dynamo magnetic field on the velocity distribution to be of fundamental interest and worth performing in the Karlsruhe test facility, since it may further elucidate the saturation mechanism in the transcritical range. In another series of dynamo experiments, we have addressed the problem that will be outlined in this article. The key experimental issue in this context is the simultaneous measurement of the local sodium velocity in the channels of the test facility and the intensity of the local magnetic field in the vicinity of the velocity probes. This paper is organized as follows. Section 2 recalls briefly the principal design of the Karlsruhe test facility and outlines the specific instrumentation. The measured results for the magnetic field, and the local velocity in the axial flow channels are presented and discussed in § 3. In the Appendix the evaluation formulae for the permanent magnet potential probe used are derived and discussed in some detail.

## 2. The test facility and its instrumentation

Stieglitz & Müller (1996) and Müller *et al.* (2004) described the Karlsruhe test facility in some detail. The test rig consists essentially of a cylindrical module which contains 52 channel-type vortex generators connected to three independent sodium loops, each of which is equipped with an MHD feed pump and a heat exchanger to ensure constant operational temperature during the experimental runs. The helical and axial channel flow in the vortex generators in terms of volumetric flow rates $\dot{V}_H$ and $\dot{V}_c$ can be independently controlled by forced flow in the different sodium loops. The structure and the principal arrangement of the vortex generators is sketched in figure 1, together with essentials of the instrumentation and a coordinate system.

The sodium volumetric flow rate in each sodium loop was measured by electromagnetic flow meters outside the test module. The pressure drop across the module channel systems was determined by capacitance pressure gauges. The dynamo magnetic field was identified by two independent sensor systems. Three Hall sensors attached to a traversable prong (two at position H3, one at position H4, see figure 1) could be moved in a borehole along the centre axis of the module, and were used to measure locally three components of the magnetic field. Two more Hall sensors were fixed at positions H5 and H6 on the module's mantle. Each Hall sensor measured

https://doi.org/10.1017/S0022112006008779 Published online by Cambridge University Press

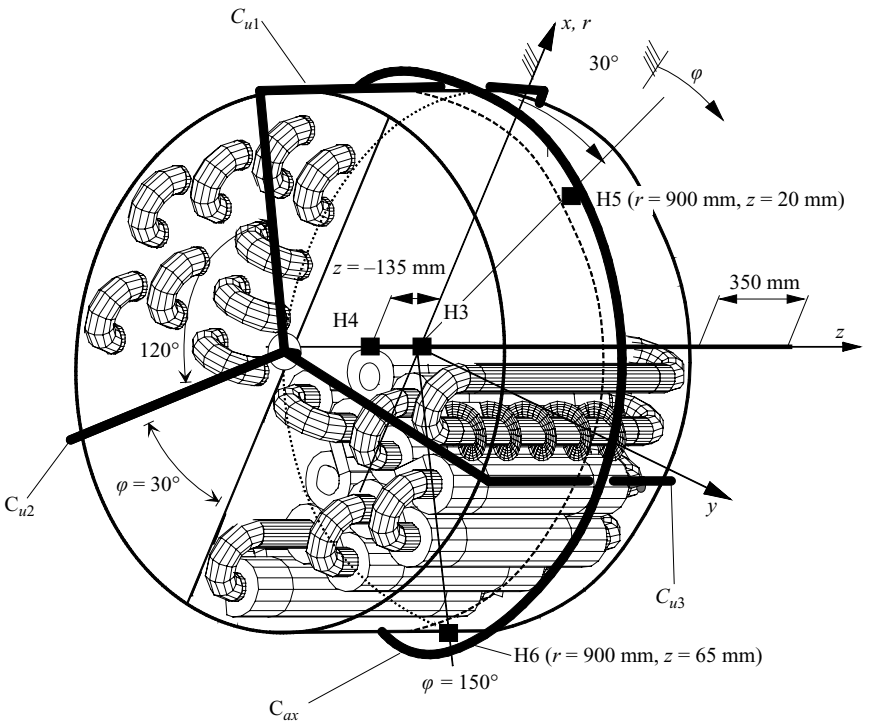



FIGURE 1. Technical sketch of the dynamo module and its instrumentation with Hall sensors and flux sensors embedded in a coordinate system. H3, two Hall sensors to measure three field components $B_x$, $B_y$, $B_z$; H4, one Hall sensor to measure $B_y$; H5, one Hall sensor to measure two components $B_z$ and the radial component $B_r$; H6, one Hall sensor to measure the radial component $B_r$; $C_{ax}$, sensor coil to measure the time rate of change of the axial magnetic flux component $\dot{\Phi}_z$; $C_{u1}$, $C_{u2}$, $C_{u3}$, sensor coils to measure the time rate of change of the azimuthal magnetic flux component$\dot{\Phi}_\varphi$.

one directional component of the magnetic field, except for two sensors at positions H3 and H5 which could record two components. Thus, at position H3, all three field components were recorded. The transient phase of onset of dynamo action as well as the dynamic behaviour of the magnetic field at constant supercritical operation could be measured through a set of sensor wire coils that are either threaded through the borehole in the module centre, or are twined around the module equator, as indicated schematically in figure 1. These sensor coils detected time variations of the overall magnetic fluxes through planes of different orientation in terms of induced voltage time series depending on the spatial arrangement of the respective coils.

The measurement of the local velocity in the channels of the dynamo module is crucial for studying the feedback of the dynamo magnetic field on the velocity. For that purpose we used a so-called compensated permanent magnet probe (CPMP). A straight compensated probe was placed in the centre of an axial channel of the module next to the axis of the cylinder, as sketched in figure 2. The specific measures for the location of the probe are given in figure 2.

The measuring principle of the miniature permanent magnet potential probe is based on Ohm's law in moving electrically conducting media. Employing this measuring principle in the environment of the dynamo magnetic field requires an

https://doi.org/10.1017/S0022112006008779 Published online by Cambridge University Press

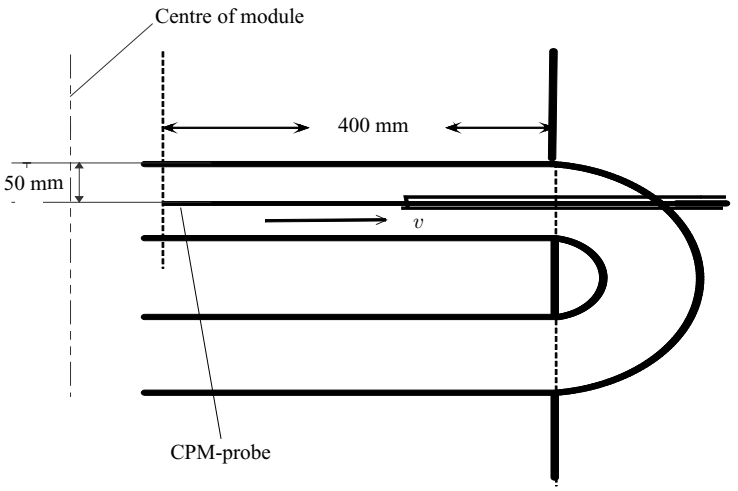



FIGURE 2. Sketch of the arrangement of the compensated permanent magnet probe (CPMP) in an axial channel of the vortex generators.

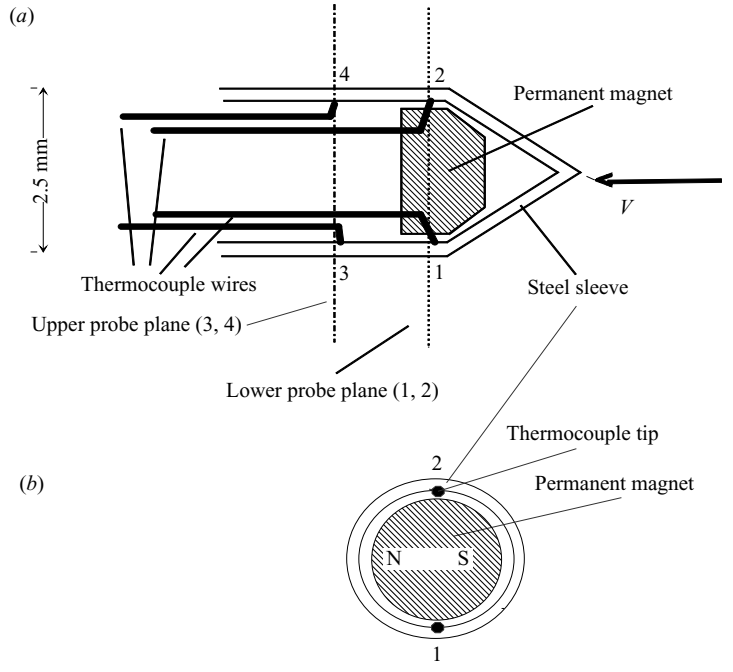



FIGURE 3. Sketch of the compensated permanent magnet probe (CPMP); (*a*) lengthwise-section, (*b*) cross-section.

evaluation procedure that eliminates the influence of the dynamo field from a measured voltage between electrical poles in the fluid. The principle of the probe and the evaluation procedure is described in the Appendix.

A sketch of the compensated permanent magnet probe (CPMP) is shown in figure 3. A miniature permanent dipole magnet of 2 mm in diameter is placed near the tip of a small stainless steel tube of 2 mm inner and 2.5 mm outer diameter. Two pairs of

https://doi.org/10.1017/S0022112006008779 Published online by Cambridge University Press

thermocouple wires (1, 2) and (3, 4) are welded to the wall inside the tube, one pair in a plane (1, 2) (dotted line 1, 2 in figure 3*a*) cutting the small dipole magnet, the other pair in another plane (3, 4) (dashed-dotted line 3, 4 in figure 3*a*) at a distance of 3 mm downstream of the first one. The attachment of the thermocouple tips at the tube walls with regard to the orientation of the magnetic dipole (indicated by 'N–S' in figure 3*b*) is such that a maximum induced voltage is recorded when liquid sodium bypasses the tip of the probe. The relationship between the velocity $u$ parallel to the probe shaft, the induced voltage $E$ between two thermocouple electrodes and the local intensity of the magnetic induction is given as $E \sim u B_\perp$ where $B_\perp$ is the component of the magnetic induction perpendicular to the two electrodes formed by a pair of thermocouples (for more details see the Appendix). We may decompose the induced voltage $E$, the velocity $u$ and the dynamo magnetic induction $B_D$ into a mean and fluctuating component that reads as $E = \bar{E} + E'$, $u = \bar{u} + u'$, $B_\perp = B_{PM} + \bar{B}_D + B'_D$ where $B_{PM}$ is the contribution of the permanent magnet to the overall magnetic induction at the probe tip.

Inserting these relationships into the relation for the induction and using simple averaging rules gives finally the evaluation equations for the temporal mean of the velocity and its fluctuation values in the form

$$\bar{u} = \gamma \frac{\bar{E}_{(12)} - \bar{E}_{(34)}}{1 - \alpha}, \tag{1a}$$

$$u' = \gamma \frac{E'_{(12)} - E'_{(34)}}{1 - \alpha}. \tag{1b}$$

The values of the factor $\gamma$ and the ratio $\alpha$ were determined from calibration measurements under subcritical, i.e. non-dynamo active flow conditions in the same test module. Details of the derivation of (1*a*) and (1*b*) and limits of their validity are outlined in the Appendix together with the calibration procedure.

## 3. Results

### 3.1. *The magnetic field*

The components of the mean dynamo magnetic induction were recorded along the positive $z$-axis of the test module, employing the traversable Hall probes. For technical reasons requiring the coolability of the Hall sensors, the probe could not be traversed beyond the centre of the axis to positions $z < 0$. A typical measured distribution of the field intensity is shown in figure 4 for equal volumetric flow rates $\dot{V}_c = \dot{V}_H = 111\,(\mathrm{m^3\,h^{-1}})$ in the axial and helical channels of the vortex generators. The data represent mean values averaged over time intervals in the range $1 < \Delta t < 3$ min at a data recording frequency of 512 Hz.

Compared to previous measurements (see Müller *et al.* 2004) the range of the recorded data has been doubled to the axial position $z = 0.60$ m which even covers a distance of 0.1 m outside the module. The more detailed measurements of the magnetic induction on the module axis can now be compared with the shape functions for the whole axial range calculated by Tilgner (2002 and personal communication) and Rädler *et al.* (2002*a*, *b*) within the scope of a kinematic dynamo model. These authors assume in their calculations a perfect cylindrical symmetry of the test module. Here we show, for simplicity, only the results of Tilgner. (For a comparison between the theoretical results of Rädler *et al.* (2002*a*, *b*) and our earlier measurements see Müller *et al.* (2004).) The graph in figure 4 confirms our conjecture from previous experiments that regarding the connecting feed-piping, (see figure 3 in Müller *et al.* 2004), the

https://doi.org/10.1017/S0022112006008779 Published online by Cambridge University Press

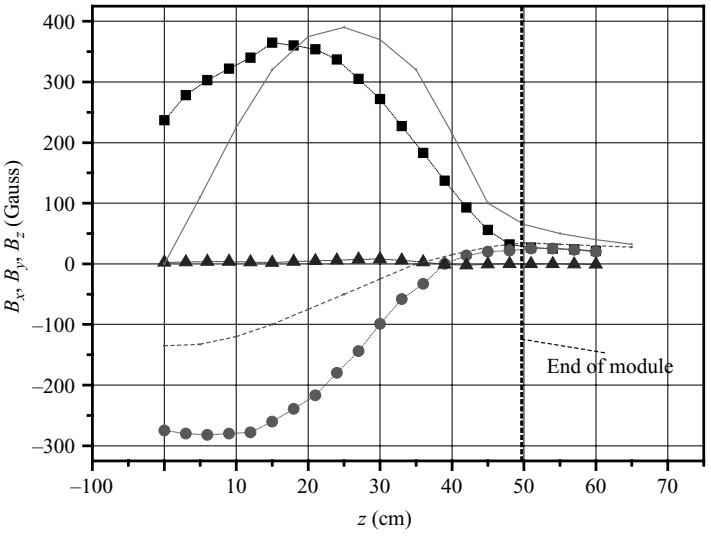



FIGURE 4. Measured components of the magnetic induction $B_x$ (■), $B_y$ (●), $B_z$ (▲) along the module axis in the range $0 \leqslant z \leqslant 0.60$ m for the volumetric flow rates $\dot{V}_c = \dot{V}_H = 111$ ($m^3\,h^{-1}$). Calculated values $B_x$ (—) and $B_y$ (- - -) from Tilgner (2002).

technical performance of the test module gives rise to an intrinsic non-symmetry of the magnetic field inside the module compared to the calculated 'symmetric' shape functions. This is best evidenced by the shift between the locations of the measured and calculated maximum $|B|$-field intensities, which for figure 4 are situated at $z = 0.14$ m and $z \approx 0.25$ m, respectively, and, moreover, by the measured finite value of $B_x$ at $z = 0$. There is a fairly good agreement between the measured and calculated field intensity in the vicinity of the module's flat wall and further outside.

Previous measurements have shown that the dynamo magnetic field is not stationary, but rather fluctuates about its mean value with significant amplitude at all recordable time scales. Figure 5 displays typical time series for the $B_y$and $B_z$ components recorded in the centre of the module (figure 5$a$, $b$) by Hall sensors, and for the time rates of change of the azimuthal and axial magnetic flux components $\dot{\Phi}_\varphi$ and $\dot{\Phi}_z$ (figure 5$c$, $d$) which were recorded by a sensor coil threaded through the borehole along the $z$-axis and inclined by an angle $\varphi = 30°$, and another one twined around the test module at the equator.

The presented records were made under strong dynamo action at equal volumetric flow rates $\dot{V}_c = \dot{V}_H = 115$ ($m^3\,h^{-1}$) in the supply loops. At first glance, all the time series in figure 5 show similar stochastic characteristics when comparing the corresponding poloidal and torroidal components. More specific features of the field fluctuation may be identified, however, from power spectral densities (PSD) associated with the time signals in figure 5. These are shown in figure 6. All displayed spectra have in common the strong power reduction in the frequency range $3 < f\,(\mathrm{Hz}) < 20$ and, generally, an even steeper decrease of power for frequencies $f > 20$ Hz. The power spectral density of $B_y$ recorded by the Hall probe shows the characteristic broadband peak centred on the frequency $f \approx 2.8$ Hz that has already been observed in previous experiments (Müller *et al.* 2004) under the same operational conditions. The power spectra in figures 6($c$) and 6($d$) for the magnetic flux components $\Phi_\varphi$ and $\Phi_z$ were obtained by time integrating the signals in figures 5($c$) and 5($d$) and a following projection

https://doi.org/10.1017/S0022112006008779 Published online by Cambridge University Press

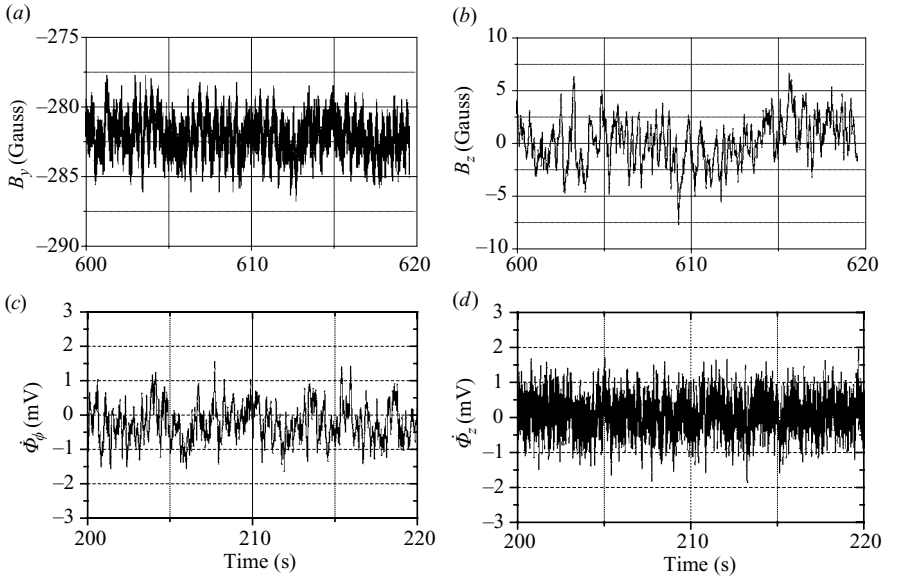



FIGURE 5. Typical time series recordings of the magnetic induction (*a*) $B_y$ and (*b*) $B_z$ measured with the Hall probe H3 at position $z = 0.075$ m (displayed in units (Gauss)) and time series of the time rate of change of the magnetic fluxes (*c*) $\dot{\Phi}_\varphi$ and (*d*) $\dot{\Phi}_z$ measured at the sensor coil $C_{u1}$ (see figure 1) for the azimuthal magnetic flux and the sensor coil $C_{ax}$ for the axial flux. (in units (μV)). Operational conditions: $\dot{V}_c = \dot{V}_H = 115$ ($m^3\,h^{-1}$).

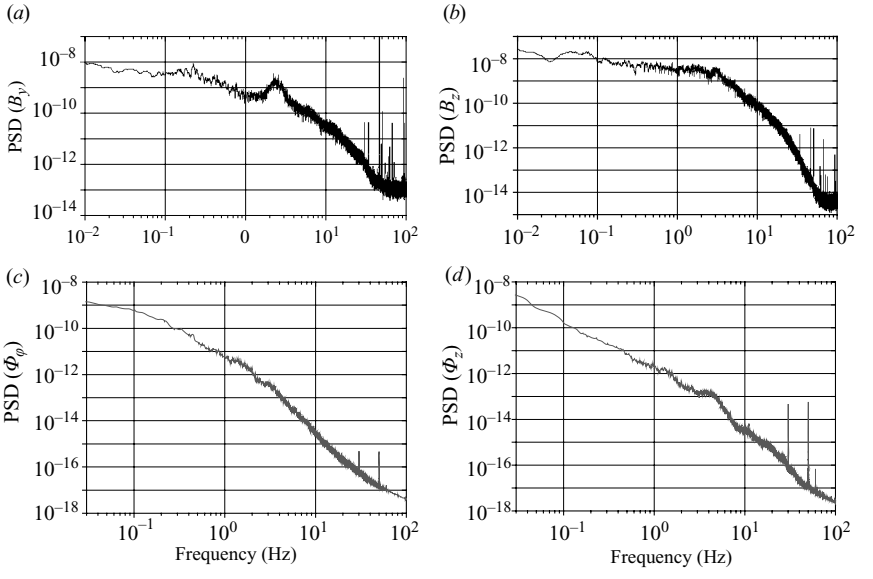



FIGURE 6. (*a*) and (*b*) power spectral densities (PSD) of time series recordings of the magnetic induction $B_y$ and $B_z$ measured with the Hall probes H3 at position $z = 0.075$ as shown in figures 5(*a*) and 5(*b*); (*c*) and (*d*) PSDs of the magnetic fluxes (*c*) $\Phi_\varphi$ and (*d*) $\Phi_z$ obtained by a time-integration of the signals in figures 5(*c*) and 5(*d*).

into the power spectral domain. They show a significantly stronger decrease in their intensity within the displayed frequency range compared to the power distribution in the spectra of the magnetic induction shown in figures 6(*a*) and 6(*b*). This indicates

https://doi.org/10.1017/S0022112006008779 Published online by Cambridge University Press

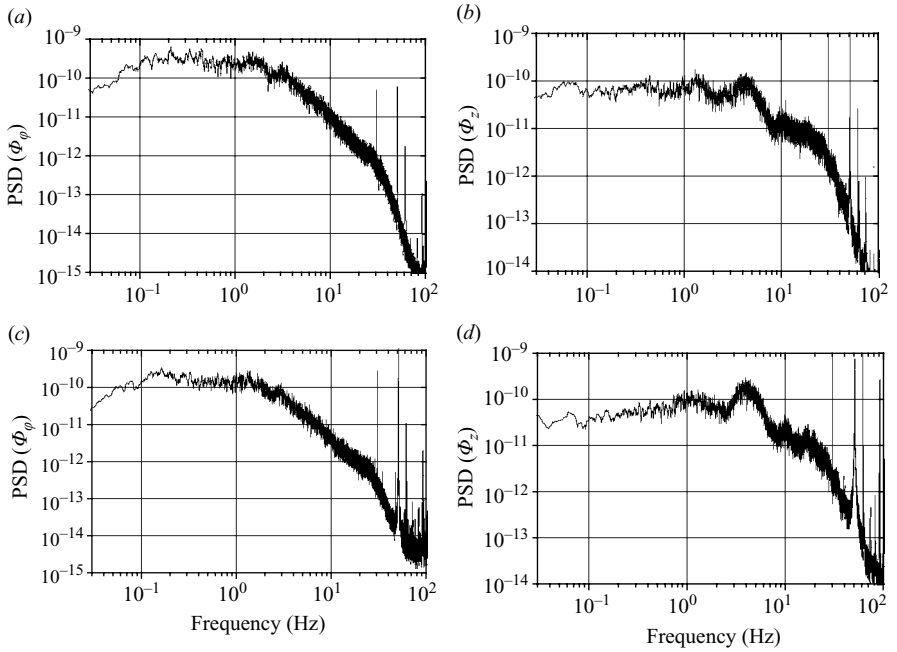



FIGURE 7. (*a*) and (*b*) power spectral densities (PSD) of the time derivatives of the magnetic fluxes $\dot{\Phi}_\varphi$ in figure 5(*c*) and $\dot{\Phi}_z$ in figure 5(*d*) for the operational conditions $V_c = V_H = 115\,(\mathrm{m^3\,h^{-1}})$, (*c*) and (*d*) PSDs of the time rate of change of the magnetic flux $\dot{\Phi}_\varphi$ and $\dot{\Phi}_z$ recorded by the poloidal and equatorial sensor coil for the operational condition $V_c = V_H = 105\,(\mathrm{m^3\,h^{-1}})$.

that the spectral power density of the magnetic induction decreases strongly from the centre to the periphery of the test module, particularly in the higher-frequency range.

The PSD-functions in figure 7 were obtained from the recorded time-signals of the sensor coils. They show two more characteristic features in the flow frequency range. (i) Another broadband peak centred around a frequency of $f \sim 4$–$5\,\mathrm{Hz}$ can be observed for the $\dot{\Phi}_z$-signal, as seen in figure 7(*b*, *d*). (ii) The PSD-functions of $\dot{\Phi}_\varphi$ obtained from an azimuthal coil, which is sensitive to temporal changes of the toroidal magnetic flux, exhibit a typical power plateau in an intermediate frequency range $0.1 < f\,(\mathrm{Hz}) < 3$ and decrease moderately towards the lower frequency range $f < 0.1\,\mathrm{Hz}$ and strongly in the higher range $f > 3\,\mathrm{Hz}$.

The specific features of the power spectral densities obtained from records of the Hall sensors near the centre of the module (figure 6*a*, *b*) match well with evaluations of previous measurements (figure 21 in Müller *et al.* 2004) and were discussed at length. Nevertheless, we would like to point out again that the broadband peak centred around the frequency $f \approx 2.8\,\mathrm{Hz}$ in the PSD-function of the $B_y$-component in figure 6(*a*) shifts to lower frequencies for decreasing intensities of the measured magnetic field, i.e. for lower volumetric flow rates. We found this power peak at $f \approx 1\,\mathrm{Hz}$ for volumetric flow rates $\dot{V}_c = \dot{V}_H = 105\,(\mathrm{m^3\,h^{-1}})$ in agreement with our earlier measurements. We conjectured previously, and still do, that this effect reflects a resonant interaction of Alfvénic fluctuations at the smallest length scale of the test module, i.e. at twice the diameter of a vortex generator. A corresponding power peak is not visible in the power spectra of the magnetic flux components $\Phi_\varphi$ and $\Phi_z$ in

https://doi.org/10.1017/S0022112006008779 Published online by Cambridge University Press

figures 6(*c*) and 6(*d*). This seems reasonable in the light of the effective short range of Alfvénic fluctuations.

As mentioned above, another distinct broadband power peak is observed in the spectra of the signals from the equatorial coil in figures 7(*b*) and 7(*d*). The equatorial coil senses the time derivative of the magnetic flux component along the module axis. The peak is centred around a frequency of $f \approx 4$–$5$ Hz. However, contrary to the spectral behaviour of the local signals by Hall sensors, the location of this power peak in the frequency domain does not change noticeably when we reduced the operational volumetric flow rates, e.g. to $\dot{V}_c = \dot{V}_H = 105\ (\mathrm{m^3\,h^{-1}})$. This is demonstrated by figure 7(*d*). We suggest that in this case the location of the power peak originates from hydrodynamic fluctuations of the swirling flow in the vortex generators that stretches and transports the mean magnetic field lines. A time scale in accord with this idea is given by the injection frequency of hydrodynamic helicity into the system. This may be defined, for example, as $f_{in} = \bar{u}_H/a\pi$ where $\bar{u}_H$ is the mean velocity in the helical channels and $a$ the diameter of the vortex generator (see the table in the Appendix of Müller *et al.* 2004). For our specific cases, this results in values $f_i \approx 4.7$ Hz for volumetric flow rates $\dot{V}_c = \dot{V}_H = 115\,(\mathrm{m^3\,h^{-1}})$, and in $f_i \approx 4.2$ Hz for the flow rates$\dot{V}_c = \dot{V}_H = 105\,(\mathrm{m^3\,h^{-1}})$. We consider this as a reasonable estimate with regard to the rough assumptions for the velocity distribution in the helical channel. Using the mean velocities in the channels instead, which are of the order of 3–4 $(\mathrm{m\,s^{-1}})$ would have resulted in a one-order-higher estimated frequency (compare table 1 in Müller *et al.* 2004). As mentioned before, the power spectra evaluated from signals recorded by the poloidal sensor coils, as depicted in figures 7(*a*) and 7(*c*), show a characteristic accumulation of power in the range of frequencies $0.1 < f\,(\mathrm{Hz}) < 1.2$ with a strong power decay to higher and a moderate power reduction to lower frequencies. We may translate this observation also into the wavenumber space by using Taylor's hypothesis and the smallest typical velocity of the system, the axial component of the mean velocity in the helical channels which is typically $\bar{u}_{H(ax)} \approx 1\,(\mathrm{m\,s^{-1}})$. The power-containing range of wavenumbers $k$ would than be $0.6 < \mathrm{k}\,(\mathrm{m^{-1}}) < 7.5$ and the associated range of wavelengths $\lambda$ would be $0.8 < \lambda(\mathrm{m}) < 10$. This suggests that the most energetic fluctuations of the dynamo magnetic field are accumulated in the large-scale field components.

All of the displayed spectra in figures 6 and 7 have in common the strong decay in the dissipative range of frequencies beyond the Kolmogorov frequency $f_{K\lambda}$ based on the magnetic diffusivity which we evaluated previously (see table 1 in Müller *et al.* 2004) and which varies for the cases considered between $9 < f_{K\lambda}\,(\mathrm{Hz}) < 15$.

Furthermore, there is a significant cross-correlation between the different components of the magnetic field measured by Hall sensors at different positions, but at a moderate distance from each other. A typical cross-correlation function (CCF) is shown in figure 8 for the supercritical conditions $\dot{V}_c = \dot{V}_H = 112\,(\mathrm{m^3\,h^{-1}})$. There is a relatively strong correlation of about 30 % between the fluctuations of the $B_y$-components measured at the locations $z = -0.06$ m and $z = 0.075$ m on the module axis.

The time signals of these $B_y$-components are correlated through a quasi-periodic fluctuation with a period of about $\tau \approx 0.4$ s. This period is compatible with the observed frequency peak in the PSD-function of the $B_y$ component in figure 6(*a*). Moreover, a delay time $\tau \approx 0.1$ s may be identified from the graph by estimating the position of the maximum of an envelope to the oscillatory CCF as $\Delta t \approx -0.1$ s (see Bendat & Piersol 1986). These two effects may be interpreted by a perturbation wave package travelling at a group velocity of about $1(\mathrm{m\,s^{-1}})$. There are at least two possible

https://doi.org/10.1017/S0022112006008779 Published online by Cambridge University Press

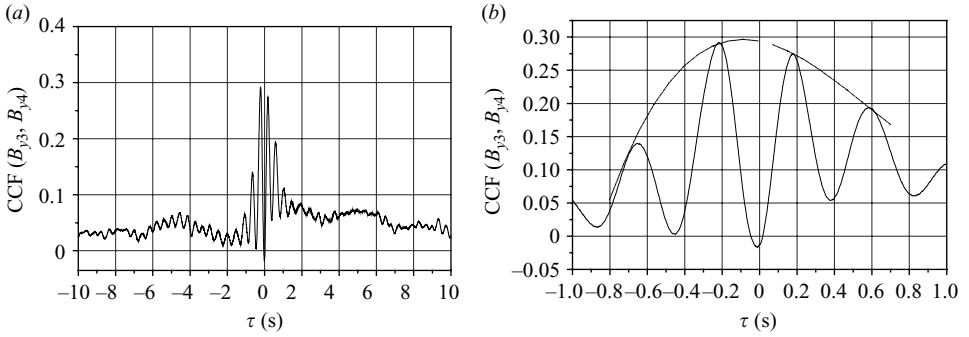



FIGURE 8. Cross-correlation functions for time signals of the $B_y$-components of the magnetic induction recorded by the Hall probes at position H3 and H4; distance between the probes: $d = 0.135\,\mathrm{m}$. Operational conditions $\dot{V}_c = \dot{V}_H = 112\,(\mathrm{m^3\,h^{-1}})$.

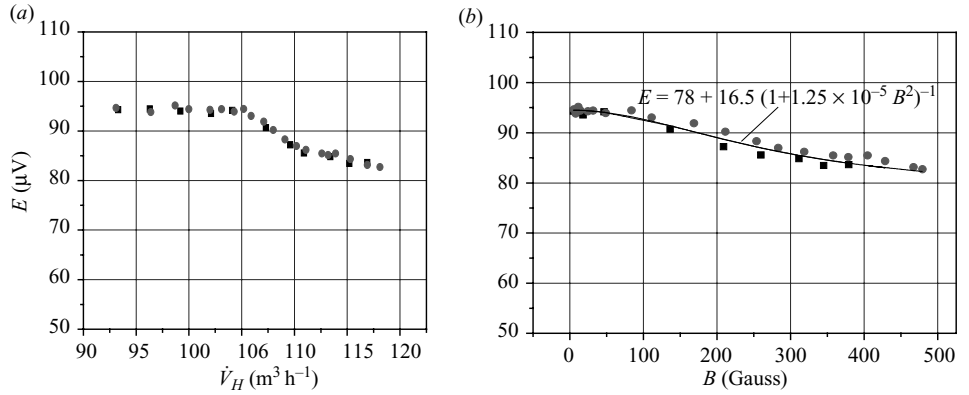



FIGURE 9. The measured compensated mean induced voltage from the permanent magnetic probe (CPMP) in the centre of an axial channel of a vortex generator next to the axis of the module (*a*) as a function of the helical flow rates at a fixed axial flow rate of $V_c = 105\,(\mathrm{m^3\,h^{-1}})$, (*b*) as a function of the local induction $B$ measured by hall probes at the location $x = 0.1\,\mathrm{m}$, $y = 0.1\,\mathrm{m}$, $z = 0.077\,\mathrm{m}$. According to calibration measurements the following relation holds: $1\,\mu V$ measured by the CPM-probe corresponds to an axial local velocity variation $\Delta u = 4.67\ \times 10^{-2}\ (\mathrm{m\,s^{-1}})$ (see Appendix). ■, ●, measurements on different days.

mechanisms for spatial correlations: (i) the radiative energy transport by Alfvén waves and (ii) the convective energy transport by the fluid flow in the channels. The first one is certainly limited to short distances because of the strong Joule damping of these waves in liquid sodium. The rate of correlation must be expected to be weak even for short distances. We thus conjecture, that the delay time of $\tau \approx 0.1\,(\mathrm{s})$ originates from a field disturbance that is transported between the two Hall-sensors in the helical flow domain by the axial component of the helical velocity. The transport velocity is associated with the volumetric helical flow rate $\dot{V}_H = 112\,(\mathrm{m^3\,h^{-1}})$ and is calculated roughly as $\bar{u}_{H(ax)} \approx 1.21\,\mathrm{m\,s^{-1}}$. The distance between the two relevant Hall-sensors was $d = 0.135\,\mathrm{m}$.

### 3.2. *Velocity characteristics due to the feedback of the dynamo magnetic field*

Figure 9 presents the measured compensated mean induced voltage $E = \bar{E}_{(12)} - \bar{E}_{(34)}$ recorded by the CPM-probe as a function of the helical flow rate $\dot{V}_H$. Figure 9(*a*) shows the influence of the dynamo magnetic field on the local mean velocity in

https://doi.org/10.1017/S0022112006008779 Published online by Cambridge University Press

the centre of an axial channel at a position $(x, y, z) = (0.1\,\mathrm{m},\ 0.1\,\mathrm{m},\ 0.075\,\mathrm{m})$. The experiments were conducted at a fixed axial flow rate of $\dot{V}_c = 105\,(\mathrm{m^3\,h^{-1}})$ and for varying helical flow rates in the range $93 < \dot{V}_H \leqslant 118\,(\mathrm{m^3\,h^{-1}})$. For subcritical conditions, i.e. $\dot{V}_H < 105\,(\mathrm{m^3\,h^{-1}})$, the local velocity, represented by the measured induced voltage, is constant. Once dynamo action sets in at higher helical flow rates, the velocity, i.e. the measured voltage, decreases first, but finally approaches saturation at a lower level for even higher helical flow rates. The maximum velocity in the channel centre at subcritical conditions is reduced by about 13 % and tends towards a plateau value at even higher supercritical states. Figure 9(*b*) demonstrates the dependency of the same effect on the intensity of the local induction of the dynamo measured by the Hall probes at position H3 (see figure 1). In this figure, the measured data were fitted by an ansatz-function in the form: $E = 78 + 16.5\,(1 + 1.25 \times 10^{-5} B^2)^{-1}$. This function corresponds in its form and in the order of magnitude of its coefficients with the 'quenching-function' that Rädler *et al.* (2002*b*) used to model the feedback effect of the deformation of the velocity profiles in the flow channels on the saturation process of the dynamo magnetic field at supercritical conditions. Thus, our experimental findings support in some way the nonlinear model for the saturation mechanism of the dynamo magnetic field of Rädler *et al.* (2002*b*).

The decrease of the local velocity with increasing helical flow rates can be explained by a transition of an ordinary turbulent velocity profile in a circular channel to a slug-type MHD velocity profile under the influence of the increasing intensity of the mean magnetic field. This magnetic field is essentially perpendicular to the channel direction and induces Lorentz forces to generate velocity redistributions. From MHD-textbooks (see e.g. Shercliff 1965; Branover 1978; Moreau 1990) it is known that a balance between pressure and Lorentz forces governs the channel flow at Hartmann numbers of several hundred and that slug type velocity profiles occur in single pipes. The achieved maximum local magnetic field intensities corresponding to figure 9 were 480 (Gauss) at a helical flow rate $\dot{V}_H = 118\,(\mathrm{m^3\,h^{-1}})$. This implies a Hartmann number $Ha \approx 600$ (for the definition of the Hartmann number we refer to table 1 of Müller *et al.* 2004). This is an order of magnitude where a core flow, i.e. slug flow approximation, may describe MHD-channel flow satisfactorily. The saturation behaviour of the velocity for high Hartmann numbers is thus obvious within the scope of an asymptotic MHD core-flow model. We mention here explicitly that the 13 % decrease of the local velocity, measured by the CPM-probe in the channel centre is in fair agreement with the relationship between the maximum turbulent velocity in a fully developed turbulent pipe flow and the associated mean flow which is $\bar{u} = 0.84\,u_{max}$ for a Reynolds number $Re = 10^6$ (see e.g. Schlichting 1958, p. 467). These facts support our explanations for the MHD-saturation process.

The response of the dynamo magnetic field to the velocity fluctuations can be identified from the r.m.s-values of the compensated time signal $E' = E'_{(12)} - E'_{(34)}$ recorded at the CPM-probe. A sequence of r.m.s.-data for subcritical and supercritical flow conditions are plotted in figure 10 for equal flow rates in the channel systems.

The data were evaluated from recordings of 20 min at a data acquisition rate of 512 Hz and for equal axial and helical flow rates. At subcritical flow rates, i.e. $\dot{V}_c = \dot{V}_H < 105\,(\mathrm{m^3\,h^{-1}})$ we observe a moderate linear increase of the r.m.s. values. When dynamo action sets in for $\dot{V}_c = \dot{V}_H \geqslant 105\,(\mathrm{m^3\,h^{-1}})$, the growth rate of the r.m.s.-values becomes suddenly larger, but levels off for even higher volumetric flow rates as is indicated by the fitting line through the data points.

At first glance, it is surprising that the velocity fluctuations and as their measure, the r.m.s.-values, grow beyond the level of ordinary turbulence fluctuations under

https://doi.org/10.1017/S0022112006008779 Published online by Cambridge University Press

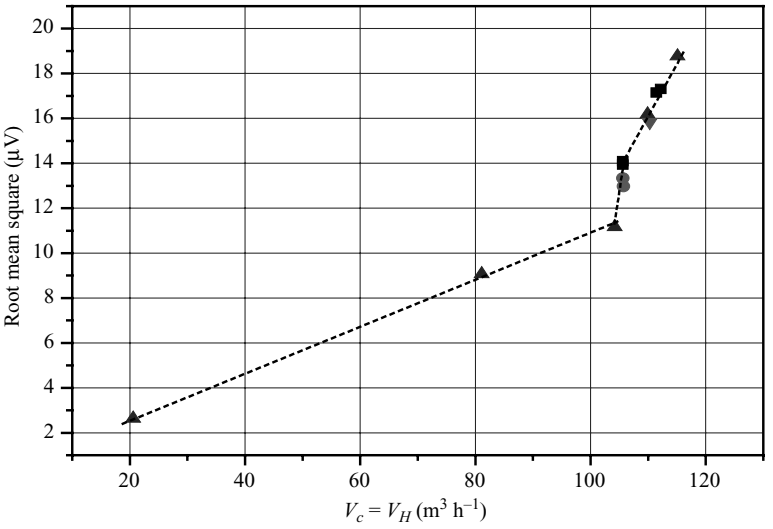



FIGURE 10. The evaluated r.m.s.-values for the axial velocity fluctuations as a function of the volumetric flow rates for conditions of equal helical and axial flow rates; ◆, ▲, ■ experimental data recorded on different days; - - - -, fitting line.

the influence of dynamo action, as figure 10 indicates. We could have speculated that because of Joule dissipation these fluctuations were dampened instead, at least in the channel centre. This has been observed for fully developed liquid-metal pipe flow under the influence of a homogeneous external magnetic field (see also the above cited text books on MHD). In our experiment, such clean conditions are not available. On the contrary, the turbulent channel flow is not fully developed only 6 pipe diameters downstream of a 180° bend and is contaminated by secondary flows originating from the bend. Moreover, the fluctuating dynamo magnetic field acts on the turbulent channel flow. Taking into account the principal spatial resolution limits of the CPM-probe and requiring a systematic error margin of less than say 5 % (see the Appendix for more discussion), this probe is capable of sensing with reasonable accuracy temporal fluctuations corresponding to vortices of wavelengths comparable with the diameter of the axial channel, i.e. $d_H = 0.1$ m. Spatial perturbations of this size correspond to fluctuation frequencies up to about 40 Hz at channel velocities of about 4 m s$^{-1}$.

Twice the channel diameter is, of course, also the natural length scale to start dynamo action in the 52 vortex generators. Thus, it is justified to assume that the increasing velocity fluctuations reflect above all the onset and further development of the dynamo excitation. A sublinear increase of the MHD-turbulence level in the range of dynamo action, seen in figure 10, seems reasonable in the light of a transcritical bifurcation process that we encounter with the onset of dynamo action (see Müller *et al.* 2004). It indicates a saturation effect also for the dynamo relevant velocity fluctuations in the lower range of length scales associated with the generation of the dynamo magnetic field.

For representative subcritical, near critical and supercritical states the power spectral densities of the compensated velocity signal are shown in figure 11. Assessing the technical quality of the PSD-functions in figure 11, we must realize that the power spectra are affected by a significant instrumental noise level as the observable power reduction is only one decade in the relevant frequency range $0.5 < f\,(\mathrm{Hz}) < 100$.

https://doi.org/10.1017/S0022112006008779 Published online by Cambridge University Press

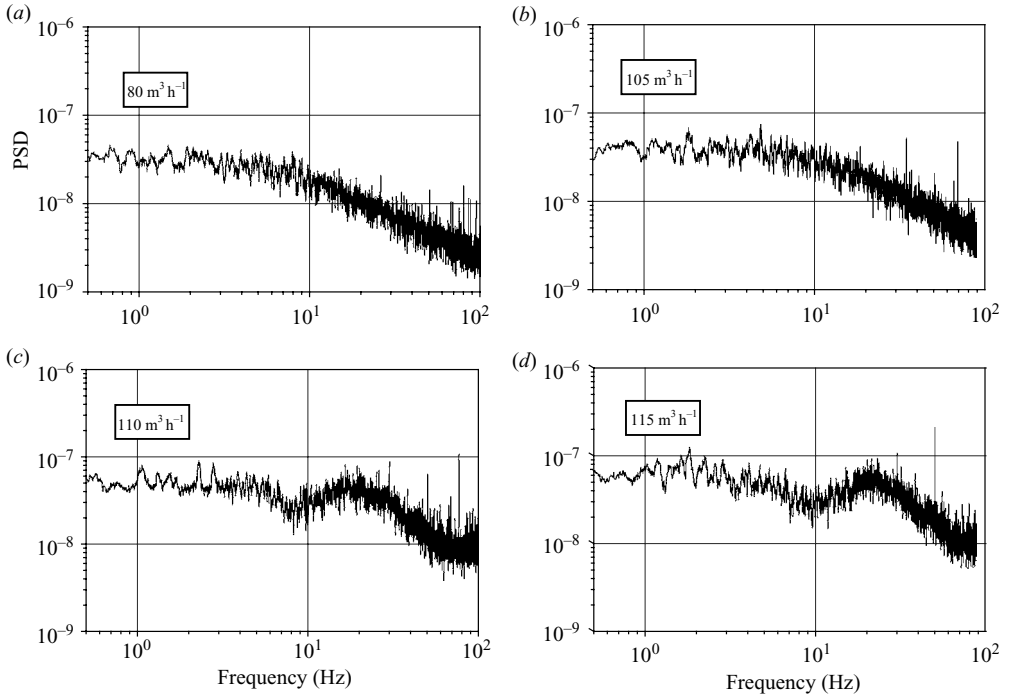



FIGURE 11. Power spectral density (PSD) for the velocity signal from the compensated permanent magnet probe (CPMP) recorded for sub critical ($\dot{V}_c = \dot{V}_H = 80\,(\mathrm{m^3\,h^{-1}})$), near critical ($\dot{V}_c = \dot{V}_H = 105\,(\mathrm{m^3\,h^{-1}})$) and supercritical ($\dot{V}_c = \dot{V}_H = 110\,(\mathrm{m^3\,h^{-1}})$; $\dot{V}_c = \dot{V}_H = 115\,(\mathrm{m^3\,h^{-1}})$) operational conditions.

Nevertheless, as a characteristic physical feature we see that the power level in the low-frequency range $0.5 < f\,(\mathrm{Hz}) < 5$ increases slightly from the subcritical to the near-critical range ($\dot{V}_c = \dot{V}_H = 80\,(\mathrm{m^3\,h^{-1}})$ to $\dot{V}_c = \dot{V}_H = 105\,(\mathrm{m^3\,h^{-1}})$) and, furthermore, in the supercritical range ($\dot{V}_c = \dot{V}_H = 110\,(\mathrm{m^3\,h^{-1}})$ to $\dot{V}_c = \dot{V}_H = 115\,(\mathrm{m^3\,h^{-1}})$). This accords with findings for the r.m.s.-values of figure 10. Indeed, an integration of the power spectra in the frequency domain resulted in variance values corresponding to the r.m.s.-values of figure 10. Furthermore, for supercritical conditions, we may recognize a spectral power shift from the lower- to the higher-frequency range. As a consequence, a stronger decay of power occurs in the observable final range, which indicates an increase of the magnetohydrodynamic dissipation for higher frequencies. There is also an intermediate frequency range $5 < f < 10\,\mathrm{Hz}$ of reduced power at supercritical conditions. A power accumulation adjoins this power suppression as seen by the broadband peak around a frequency $f \approx 20\,\mathrm{Hz}$. This observation indicates an obviously non-uniform, selective amplification or damping mechanism for the velocity fluctuations in the higher-frequency domain under the influence of dynamo action.

The power decay in the high-frequency range $10 < f\,(\mathrm{Hz}) < 100$ follows fairly well an $f^{-1}$ power law in the sub- and near-critical range and an $f^{-1.5}$ power law in the supercritical range. For fully developed turbulent pipe flow we expected, as outlined in Müller *et al.* (2004), the Kolmogrov (1941) spectral distribution $E_f^V \sim f^{-5/3}$ for the inertial subrange at subcritical condition and a generalized (Iroshnikov 1964; Kraichnan 1965; Biskamp 1993) energy spectrum for correlated MHD-turbulence in the form $E_f^V \sim f^{-m}$ with $3/2 < m < 3$. This is not the case for the

https://doi.org/10.1017/S0022112006008779 Published online by Cambridge University Press

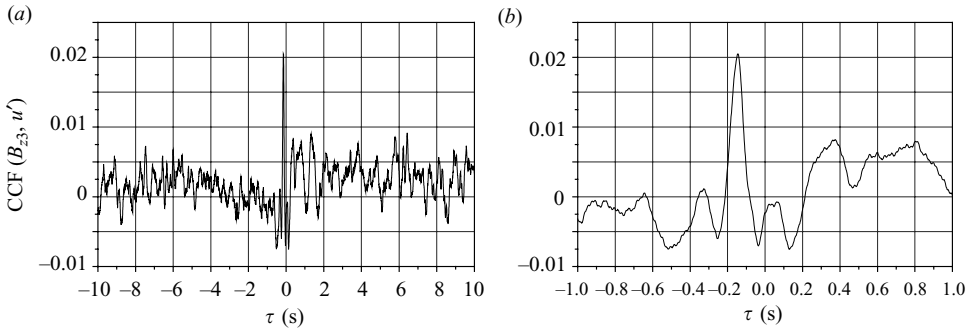



FIGURE 12. Normalized cross-correlation function (CCF) of the velocity signal recorded by the compensated permanent magnet probe at position (0.1, 0.1, 0.075 m) and the signal of a Hall probe for $B_z$ at position (0, 0, 0.075 m). The CCFs are presented for two temporal reductions ($-10 < t\,(\mathrm{s}) < 10$) and ($-1 < t\,(\mathrm{s}) < 1$). Operational conditions: $\dot{V}_c = \dot{V}_H = 115\,(\mathrm{m^3\,h^{-1}})$.

hydrodynamic turbulence in our axial channel flow which is not fully developed. For the magnetohydrodynamic turbulence, only the lower limit of the generalized power law seems to have been realized. We attribute this deficit in part to the too small signal to noise ratio of about 10 of the measuring chain of the CPM-probe. As a consequence, our former interpretations (Müller *et al.* 2004) of the observed strong spectral power decay of the magnetic energy, as displayed in the PSD-graphs in figure 6, cannot be based on our present experimental findings.

Another challenging aspect of dynamo action is the mutual influence between fluctuations of the magnetic field and the velocity. We investigated this issue by cross-correlating the time signals of the CPM-probe with those of the Hall and coil sensors for different components of the magnetic induction and time derivatives of the magnetic flux, respectively, and for various operational states. We found relevant correlations between the signals only for short distances between the locations of the probes, for short time scales of the order of less than 1 s and under conditions for the largest technically feasible dynamo magnetic fields of several hundred Gauss. A typical example for a cross-correlation between the time signal for the velocity from the CPM-probe at a position $x = 0.1$ m, $y = 0.1$ m, $z = 0.075$ m and a signal of the $B_z$-component from a Hall sensor at position $x = 0$, $y = 0$, $z = 0.075$ m is shown in figure 12.

The operational conditions were $\dot{V}_c = \dot{V}_H = 115\,(\mathrm{m^3\,h^{-1}})$. The correlation graph shows two characteristic features. (i) A small, nevertheless, distinct 2 % correlation of a quasi-periodic fluctuation of a period of about $\tau_P \approx 0.2$ s. (ii) A time delay of $\tau_d \approx -0.15$ s. According to Bendat & Piersol (1986), the quality of the CCF in figure 12 may be associated to narrowband random noise signals. The same quality of correlation was also observed for a state of operation with $\dot{V}_c = \dot{V}_H = 112\,(\mathrm{m^3\,h^{-1}})$, however, not for even lower flow rates. No significant correlations could be identified between the other two components of the magnetic induction $B_x$, $B_y$ and the velocity from the corresponding time signals under the same flow rate conditions.

The cross-correlations between the time signals of the coil sensors (see figure 1) and the CPM-probe showed similar features. Two typical CCF-examples for the time derivatives of an axial and an azimuthal magnetic flux and the axial velocities are shown in figure 13. The operational conditions were the same as in figure 11 for $\dot{V}_c = \dot{V} = 115\,(\mathrm{m^3\,s^{-1}})$. The 'equator'-coil measured the time rate of change of the axial flux $\dot{\Phi}_z$. The signal of $\dot{\Phi}_\varphi$ was recorded by a coil in a plane inclined by an angle

https://doi.org/10.1017/S0022112006008779 Published online by Cambridge University Press

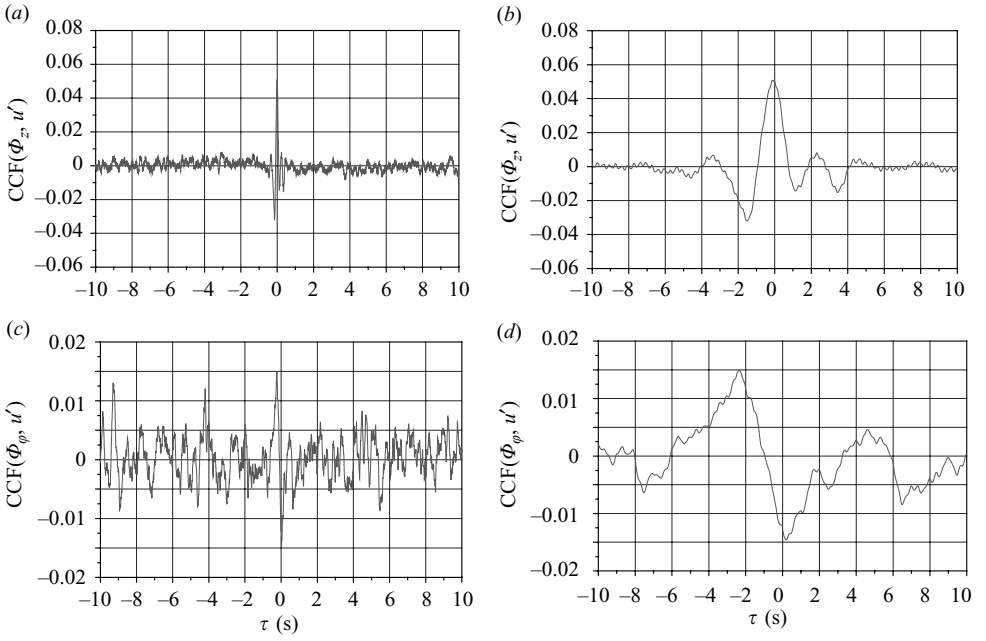



FIGURE 13. Cross-correlation functions (CCF) of the velocity signal recorded by the compensated permanent magnet probe 1 at position (0.1, 0.1, 0.075 m) and signals of the coil flux sensors $C_{ax}$ $(a, b)$ and $C_{u1}$ $(c, d)$ for the axial and azimuthal magnetic flux components. Each CCF is presented for two different time intervals $(-10 < t\,(\mathrm{s}) < 10)$ and $(-1 < t\,(\mathrm{s}) < 1)$. Operational condition: $\dot{V}_c = \dot{V}_H = 115\,(\mathrm{m^3\,h^{-1}})$.

of 30° to the $(x, z)$-coordinate plane (see figure 1). In figure 13$(a, b)$ a correlation of about 5 % is seen between the axial magnetic flux and the velocity in the axial channel. Moreover, there is a strongly dampened, quasi-periodic correlation signal for a time interval $|\Delta t| < 0.4$ s with a period of about $\tau_P \approx 0.2$ s in accord with the observation for the correlation between the Hall- and the CPM-probe signals in figure 12. However, a noticeable time delay does not exist in this case, in contrast to the correlations between the Hall- and CPM-probe signals. Furthermore, a significant correlation between the measured time derivative of the azimuthal magnetic flux and the axial velocity cannot be identified from figure 13$(c, d)$. This is in accordance with the observation for correlations between the $B_y$, $B_x$-components and the axial velocity.

The evaluations of the spatial cross-correlations between the velocity and magnetic field fluctuations presented in figures 12 and 13 show a distinct preference for an interaction of fluctuations of the co-oriented axial velocity $u_z$ and induction component $B_z$. This holds for the time series recorded by the Hall and coil sensors. This may be interpreted as coherence between the axial velocity fluctuations and the stretching of mean radial magnetic lines of force by just these velocity fluctuations. The quasi-periodic character of this coherency at a period of roughly $\tau_P \approx 0.2$ s underlines the hydrodynamic origin for this observation. This time period is compatible with the injection frequency for the hydrodynamic helicity into the system referred to above. The readable delay time between the correlated signals in figure 12$(b)$ is $\tau_d \approx 0.15$ s. Two transport mechanisms for the magnetic field offer an explanation for the observed delay time of the cross-correlation, namely Alfvén waves and magnetic diffusivity.

https://doi.org/10.1017/S0022112006008779 Published online by Cambridge University Press

For our specific arrangement of the two probes, the distance between them was 0.14 m. The Alfvén velocity based on the measured intensity of the mean magnetic field is $V_A \approx 1\,(\mathrm{m\,s^{-1}})$. This corresponds to a transport time of 0.14 s for an Alfvénic fluctuation to travel between the two sensors, a value very close to the measured delay time of 0.15 s. If we choose diffusion, described by the magnetic diffusivity $\lambda = 0.1\,(\mathrm{m^2\,s^{-1}})$, as the governing transport process between the sensors, then this would result in a delay time of 0.2 s, a value slightly higher than that observed. Considering the two possible explanations and the closeness of the derived relevant transport times, the present data base does not provide a conclusive preference for one of them. The governing transport process for the fluctuations of the magnetic field under supercritical dynamo conditions requires, therefore, further investigations.

The fact that we could not detect any significant delay time from cross-correlation measurements employing the CPM-probe and the equatorial coil sensor (see figure 13*a*, *b*) must be attributed to the integrating effect of the coil sensor with regard to the flow in all 52 helical channels having a vanishing overall hydrodynamic helicity.

## 4. Conclusions

The presented experimental results complement and extend previous experimental investigations (Müller *et al.* 2004) in two respects.

Extending the measurements of the magnetic field components along the test module axis from the centre to a distinct location outside of the module specified furthermore the properties of the mean dynamo magnetic field. The measured data indicate an intrinsic non-symmetric field distribution in the real test module, compared to calculated data obtained for an ideal symmetric test. The dynamic behaviour of the magnetic field was explored in addition by a signal analysis for the time rate of change of the azimuthal and axial dynamo magnetic flux obtained from sensor coils. The power spectra of the temporal variations of the azimuthal flux show a power accumulation in an intermediate low-frequency range that corresponds to large spatial scales of the magnetic field. The power spectra of the axial flux variations reveal the injection of mechanical helicity into the system by a power peak at a frequency that is compatible with the turn-around time of the flow in the helical channels.

The back reaction of the dynamo magnetic field on the velocity distribution in the axial channels of the test module was analysed with the help of a compensated permanent-magnet-potential-probe. The evaluation of the mean values of the probe signals indicates a transition of a turbulent hydrodynamic pipe flow velocity profile into a magnetohydrodynamic slug-flow profile for increasing dynamo intensities. The measured local turbulent intensities of the velocity increase with the onset of dynamo action but exhibit a trend to saturation at pronounced supercritical conditions. This contrasts at first glance with the common experience that turbulent fluctuations are dampened in fully developed MHD-channel-flow owing to the additional Joule dissipation. However, the effect of the fluctuating inhomogeneous dynamo magnetic field on velocity perturbations leads to a different observation. A significant cross-correlation exists between the time signals of the axial component of the dynamo magnetic field and the velocity in the axial channels for short spatial separation of the sensors. It is suggested that this interaction is caused by the axial convective transport of perturbations of the mean magnetic field generated by the helical flow components in the vortex generators.

https://doi.org/10.1017/S0022112006008779 Published online by Cambridge University Press

The authors thank F. H. Busse, A. Tilgner and K. H. Rödler for their continuous interest in this work and for many fruitful discussions. They have appreciated the critical and constructive comments of the reviewers.

## Appendix. The permanent magnet probe and its calibration

The measuring principle of the miniature permanent magnet probe (PMP) is based on Ohm's law in moving conducting liquids in the form

$$\boldsymbol{j} = \sigma[\boldsymbol{E} + \boldsymbol{u} \times \boldsymbol{B}], \tag{A 1}$$

where $\boldsymbol{j}$ is the electric current density, $\boldsymbol{E}$ the electric field, $\boldsymbol{B}$ the magnetic induction, $\boldsymbol{u}$ the velocity of the moving liquid and $\sigma$ the electrical conductivity of the liquid. It has been shown at length by Ricou & Vives (1982), Weissenfluh (1985) and Kapulla *et al.* (2000) that in liquid-metal flow, such as liquid-sodium flow, the current density $\boldsymbol{j}$ in relationship (A 1) can be neglected in the vicinity of small immersed test probes containing a miniature permanent magnet. This even holds, as they show, if other current sources such as thermally induced Seebeck-potentials in thermally stratified liquid-metal flows are present. Moreover, Weissenfluh (1985) has first demonstrated that in turbulent liquid-metal flow, fluctuating velocity signals can be recorded and statistically evaluated with the aid of a miniature permanent magnet probe. Horanyi & Krebs (1988), Knebel & Krebs (1994) and Knebel *et al.* 1998) developed the original concept of the probe with one miniature permanent magnetic dipole and one pair of thermocouple wires as two electrodes further on into a compensated permanent magnet probe (CPMP) with two pairs of thermocouple wires, i.e. two pairs of electrodes, as sketched in figure 3. They used this probe to measure simultaneously and directly local velocity and temperature time series in thermally stratified sodium flow. We have used their measuring and signal evaluation technique to determine the properties of the axial velocity component of a turbulent channel flow embedded in a magnetically stratified environment caused by dynamo action.

Prerequisite for an application of a permanent magnet potential probe in a magnetically stratified environment is again a negligible current density in Ohm's law, which may be modified by the external dynamo magnetic field $B_D$. The relative change of the current density owing to the dynamo field can be estimated by decomposing the current density into two parts $\boldsymbol{j} = \boldsymbol{j}_{iPM} + \boldsymbol{j}_D$ originating from the presence of the permanent magnet, the induced current $j_{iPM}$, and from the dynamo field $B_D$, the current $j_D$. Next, applying Ampere's law gives $\boldsymbol{j} = (1/\mu)\nabla \times [\boldsymbol{B}_{iPM} + \boldsymbol{B}_D]$, where $B_{iPM}$ is the induced magnetic induction due to the presence of the permanent magnetic dipole and the liquid metal flow. The relative magnitude of the two current constituents can be seen by an order of magnitude estimation using the relevant length scales for the probe, the diameter of the probe tip $d_{PM} = 2.5\,\mathrm{mm}$, the dynamo module height $h_D = 1\,\mathrm{m}$ and the hydraulic diameter of the flow channels $d_H = 0.1\,\mathrm{m}$. Furthermore, the magnetic induction may be scaled by the intensity of the miniature dipole magnet $|B_{PM}|$. We find for an estimate

$$\frac{|j|}{|B_{PM}|} < \frac{|j_{iPM}|}{|B_{PM}|} + \frac{|j_D|}{|B_{PM}|} = O\left\{\frac{1}{d_{PM}\mu}\left[\frac{|B_{iPM}|}{|B_{PM}|} + \frac{|B_D|}{|B_{PM}|}\frac{d_{PM}}{L}\right]\right\}, \tag{A 2}$$

where $L$ is one of the two relevant dynamo length scales. From this relationship, it becomes obvious that the augmentation of the current density due to the dynamo magnetic field is small as long as $|B_D|/|B_{PM}| \leqslant 1$ and $d_{PM}/L \ll 1$ as in our case namely of the order $10^{-2}$–$10^{-3}$ depending on whether the channel diameter $d_H$ or

https://doi.org/10.1017/S0022112006008779 Published online by Cambridge University Press

the module dimension $h_D$ is chosen as the relevant relevant length scale. Thus, in a good approximation the permanent magnet probe should, in principle, also work in a moderately stratified magnetic environment and the evaluation rule,

$$\boldsymbol{E} = -\boldsymbol{u} \times \boldsymbol{B}, \tag{A 3}$$

should hold in a good approximation even if $B_D$ varies in time in a moderate frequency range.

For a permanent magnet probe designed as seen in figure 3 and placed in an axial channel flow, the potential difference $E_{12}$ measured between two electrodes (1, 2) will give

$$E_{(12)} \sim u B_\perp, \tag{A 4}$$

where $B_\perp$ is the local component of the magnetic field perpendicular to the velocity component $u$ to be measured and perpendicular to a straight line between the electrodes. As $B_\perp$ is not known exactly, nor are the particular small-scale fabrications uncertainties of the probe, the probe must be calibrated under well-known flow conditions to obtain the probe characteristic in terms of a relationship

$$u = \gamma E_{(12)},$$

with $\gamma$ as the calibration factor.

We next apply relationship (A 4) to the specific design of the compensated permanent magnet probe (CPMP) and derive relationships for a direct evaluation of the time averaged mean velocity $\bar{u}$ and the velocity fluctuation $u'$. We decompose the induced voltage $E$ between two electrodes, the velocity $u$ and the dynamo magnetic induction $B_D$ in a temporal mean and a fluctuating component that read as $E = \bar{E} + E'$, $u = \bar{u} + u'$, $B_\perp = B_{PM} + \bar{B}_D + B'_D$ where $B_{PM}$ is the contribution of the permanent magnetic dipole to the overall magnetic induction at the probe tip. Inserting these relationships into relationship (A 4) and using simple averaging rules, we obtain for the voltage at the electrodes in the plane (1.2) (see figure 3).

$$\bar{E}_{(12)} \propto \bar{u}_{(12)} B_{PM(12)} + \overline{u'_{12} B'_{D(12)}} + \bar{u}_{(12)} \bar{B}_{D(12)}, \tag{A 5a}$$

$$E'_{(12)} \propto u'_{(12)} B'_{D(12)} - \overline{u'_{(12)} B'_{D(12)}} + \bar{u}_{(12)} B'_{D(12)} + u'_{(12)} B_{PM(12)}. \tag{A 5b}$$

Corresponding relationships hold for the pair of electrodes in the plane (3, 4):

$$\bar{E}_{(34)} \propto \bar{u}_{(34)} B_{PM(34)} + \overline{u'_{(34)} B'_{D(34)}} + \bar{u}_{(34)} \bar{B}_{D(34)}, \tag{A 6a}$$

$$E'_{(34)} \propto u'_{(34)} B'_{D(34)} - \overline{u'_{(34)}) B'_{D(34)}} + \bar{u}_{(34)} B'_{D(34)} + u'_{(34)} B_{PM(34)}. \tag{A 6b}$$

Because of the short distance of 3 mm between the two pairs of electrodes in the planes (1, 2) and (3, 4), we may assume that the relevant mean and fluctuating parts of the velocity and the induced dynamo magnetic field are the same in the two planes, i.e. $\bar{u}_{(12)} = \bar{u}_{(34)}$, $\bar{B}_{D(12)} = \bar{B}_{D(34)}$, $B'_{D(12)} = B'_{D(34)}$. This assumption is correct to the order $d_{PM}/L$ where $d_{PM}$is the distance between the two electrodes of the probe and $L$is either the length of the axial channel $h_D$ or its width $d_H$, if variations of the relevant quantities on the latter length scale are to be taken into account. This can be shown by a straight forward Taylor expansion of the quantities in the plane (3, 4). With these assumptions we form the difference of equations (A 5$a$) and (A 6$a$) as well as that of (A 5$b$) and (A 6$b$). We arrive, after some algebra, at the following expressions for the mean and fluctuating velocities

$$\bar{u} \propto \frac{\bar{E}_{(12)} - \bar{E}_{(34)}}{B_{PM(12)} - B_{PM(34)}}, \tag{A 7a}$$

https://doi.org/10.1017/S0022112006008779 Published online by Cambridge University Press

$$u' \propto \frac{E'_{(12)} - E'_{(34)}}{B_{PM(12)} - B_{PM(34)}}, \tag{A 7b}$$

where $B_{PM(12)}$ and $B_{PM(34)}$ are the intensities of the magnetic induction of the permanent magnet in the respective measuring plane of the pairs of electrodes. $B_{PM(12)}$ and $B_{PM(34)}$ differ significantly from each other as the effective range of the miniature dipole magnet in the probe tip is very small. The relationships (A 7*a*) and (A 7*b*) are correct to the order $d_{PM}/L$ as outlined above.

Introducing the ratio of the induction intensities $\alpha = B_{PM(34)}/B_{PM(12)}$ and a proportionality factor $\gamma$, the evaluation relationships (A 7) for the velocities to be measured by the compensated permanent magnet probe read as

$$\bar{u} = \gamma \frac{\bar{E}_{(12)} - \bar{E}_{(34)}}{1 - \alpha}, \tag{A 8a}$$

$$u' = \gamma \frac{E'_{(12)} - E'_{(34)}}{1 - \alpha}. \tag{A 8b}$$

The values of the factor $\gamma$ and the ratio $\alpha$ can be determined from calibration measurements under subcritical, i.e. non-dynamo active flow conditions.

We mention here explicitly, but do not outline in detail, that the design of the CPM-probe and its particular evaluation procedure eliminates also in principle any significant influence of the induced currents between the electrodes (12) and (34) originating from the dynamo magnetic field. This is easily seen, if the outlined evaluation procedure is directly applied to (A 1). Again, the systematic evaluation error for the CPM-probe as a whole is of the order $0.3\,\% < d_{PM}/L < 3\,\%$ depending on the relevant dynamo length scales.

For the velocity fluctuations, the CPM-probe acts as a low-pass filter, i.e. length scales smaller than the electrode-distance of 3 mm (see figure 3) cannot be resolved. To be conservative, by-passing vortices of a wavelength of 0.01 m should be sensed by the probe tip. Since the velocity in the axial channels of the test module varied in the range $3.8\,\mathrm{m\,s^{-1}} \leqslant u \leqslant 4.1\,\mathrm{m\,s^{-1}}$ for the relevant dynamo experiments, a significant deterioration of the dynamical sensitivity of the probe must only be expected in a frequency range $f > 300\,\mathrm{Hz}$. This is beyond the range of our observed relevant dynamical phenomena outlined in § 3.2. Thus, there is no significant limitation of the CPM-probe in its frequency response for our experimental applications.

Next we describe the calibration procedure of the CPM-probe. The calibration and testing of the compensated permanent magnet probe was carried out at fully installed conditions and for subcritical flow rates, i.e. without dynamo action. The compensated CPM-probe was located in the centre of an axial channel at a distance of $l = 0.56\,\mathrm{m}$ from the exit of a return bend.

For several fixed volumetric flow rates, the signals of the induced potential $E$ was recorded from the ends of the two pairs of thermocouple wires of the probe (see figure 3). (The volumetric flow rates in the axial channels of the module were measured by EM-flow meters outside the test module, as described by Stieglitz & Müller 1996).

A typical calibration record for two pairs of alumel thermocouple wires in a plane (1, 2) and (3, 4) of the CPM-probe is given in figure 14.

There is a linear relation between the measured voltage $E$ and the volumetric flow rates in the form $E = A + B\dot{V}_c$, where $A$ defines the offset and $B$ is the calibration factor. From several calibration runs we found for the parameters of the alumel wires in plane (1, 2): $B_1 = (1.114 \pm 0.02)\,(\mu\mathrm{V}/(\mathrm{m^3\,h^{-1}}))$. The respective value for the alumel wire pair in plane (3, 4) is: $B_2 = (0.210 \pm 0.003)\,(\mu\mathrm{V}/(\mathrm{m^3\,h^{-1}}))$. The overall estimated

https://doi.org/10.1017/S0022112006008779 Published online by Cambridge University Press

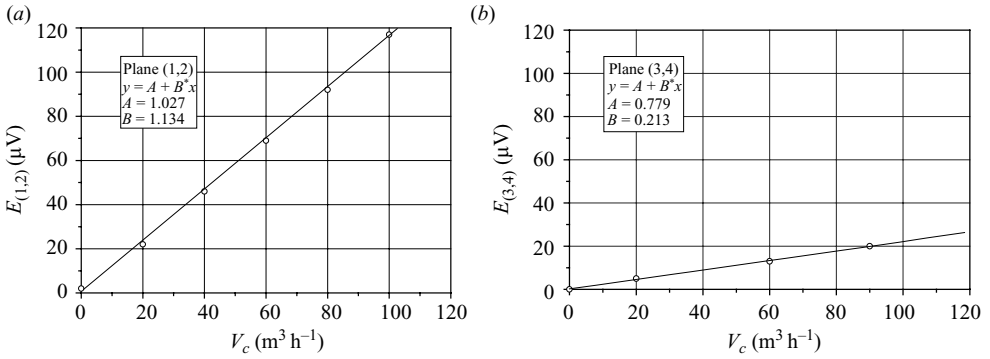



FIGURE 14. Calibration graph correlating induced voltages of CPM-probe ($E$) and volumetric flow rates $\dot{V}_c$ in the axial channels.

inaccuracy (caused by the design of the PM probe sensor, the electrical amplifier, and the volumetric flow detection) is less than 5 %. Assuming that the channel flow is quasi-fully developed in the centre of the channel we may use the relationship $\bar{u} = 0.84 u_{max}$ between the average velocity and the maximum velocity for turbulent flow in a circular pipe (see e.g. Schlichting (1958) to correlate $B$ even to the local mean velocity at the location of the probe tip.

The offset value that is primarily caused by the status of the measuring chain varied between the different runs. No uniformly valid value could be determined by calibration tests and thus had to be evaluated specifically in separate experiments. Introducing the offset corrected measured voltage in plane $(1,2)$ and plane $(3,4)$ into the relationship $E_{corr} = B\dot{V}_c$ and using the calibration factors $b_1$ and $b_2$ we obtain for the volumetric flow rate sensed by the compensated PM-probe in the centre of the axial channel (diameter $d = 0.1\,\mathrm{m}$)

$$\dot{V}_c = (\mathrm{m^3\,h^{-1}}) = \frac{1}{B_1}\frac{\bar{E}_{(12)} - \bar{E}_{(34)}}{(1 - B_2/B_1)} = 1.10\left(E_{(12)} - E_{(34)}\right)\frac{(\mathrm{m^3\,h^{-1}})}{(\mu V)}. \tag{A 9}$$

Assuming fully developed turbulent channel flow and relating the volumetric flow rate to the average channel velocity (with $1\,(\mathrm{m^3\,h^{-1}}) \div 3.55 \times 10^{-2}\,(\mathrm{m\,s^{-1}})$) this yields for the maximum velocity in the channel centre,

$$u_{max}(\mathrm{m\,s^{-1}}) = 4.67 \times 10^{-2}\left(E_{(12)} - E_{(34)}\right)\frac{(\mathrm{m\,s^{-1}})}{(\mu V)}. \tag{A 10}$$

In summary, the measurement of the velocity with the help of the compensated permanent magnet probe is flawed, with errors originating from the design of the probe, from the signal transfer in the measuring chain, and from variations in the power control of the pumps in the supply loops. The former errors were estimated as of the order $d_{PM}/L < 0.03$, the frequency resolution of flow perturbations holds up to 0.3 kHz and the sensitivity of the measuring chain is assessed as $\Delta E \approx 0.1\,\mu\mathrm{V}$. The uncertainty in the power control of the MHD-pumps amounted to an error in the volumetric flow rates of $\Delta\dot{V}/\dot{V} = \pm 0.02$. This is also reflected in the uncertainty bounds of the calibration factors $B_1$ and $B_2$ given in the text above. Thus, assessing the overall relative error of our evaluated velocity data at about 5 % seems to be reasonable.

https://doi.org/10.1017/S0022112006008779 Published online by Cambridge University Press

## REFERENCES


Bendat, J. S. & Piersol, A. G. 1986 *Random Data Analysis and Measurement Procedures*. Wiley-Interscience.

Biskamp, D. 1993 *Nonlinear Magnetohydrodynamics*. Cambridge University Press.

Branover, H. 1978 *Magnetohydrodynamic Flow in Ducts*. John Wiley.

Busse, F. H. 1992 Dynamo theory of planetary magnetism and laboratory experiments. In *Evolution of Dynamical Structures in Complex Systems* (ed. R. Friedrich & A. Wunderlin), 359–384. Springer.

Busse, F. H. 2000 Homogeneous dynamos in planetary cores and in the laboratory. *Annu. Rev. Fluid Mech.* **32**, 838–903.

Cardin, P., Brito, D., Jault, D., Nataf, H.-C. & Masso, J.-P. 2002 Towards a rapidly rotating liquid sodium dynamo experiment. *Magnetohydrodynamics* **38**, 177–189.

Chossat, P., Armbruster, D. & Oprea, I. 2001 *Dynamo and Dynamics, a Mathematical Challenge*. NATO Science Series, Kluwer.

Gailitis, A., Lielausis, O., Dement'ev, S., Platacis, E., Cifersons, A., Gerbeth, G., Gundrum, T., Stefani F., Christen, M., Hänel, H. & Will, G. 2000 Detection of a flow induced eigenmode in the Riga dynamo facility. *Phys. Rev. Lett.* **84**, 4365–4369.

Gailitis, A., Lielausis, O., Karasev, B. G., Kinlov, L. R. & Ogorodnikov, A. P. 1989 The helical MHD-dynamo. In *Liquid Metal Magnetohydrodynamics* (ed. J. Lielpetris & R. Moreau), pp. 413–419. Kluwer.

Gailitis, A., Lielausis, O., Platacis, E., Gerbeth, G. & Stefani, F. 2001 The Riga dynamo experiment. In *Dynamo and Dynamics, & Mathematical Challenge*. (ed. P. Chossat, D. Armbruster, & I. Oprea), pp. 9–24. NATO Science Series, Kluwer.

Gailitis, A., Lielausis, O., Platacis, E., Gerbeth, G. & Stefani, F. 2002 Laboratory experiments on hydromagnetic dynamos. *Rev. Mod. Phys.* **74**, 973–990.

Glatzmaier, G. A. & Roberts, P. H. 2002 Geodynamo, theoy and simulations. *Rev. Mod. Phys.* **72**, 1081–1123.

Herzenberg, A. 1958 Geomagnetic dynamos. *Phil. Trans. R. Soc. Lond.* A **250**, 543–585.

Horanyi, S. & Krebs, L. 1988 Temperature compensated miniature permanent magnet flow-meter. *First World Conference on Experimental Heat Transfer, Fluid Mechanics and Thermodynamics, Dubrovnik, September 4–9, 1988*.

Iroshnikov, P. S. 1964 Turbulence of a conducting fluid in a strong magnetic field. *Sov. Astron.* **7**, 566–571.

Kapulla, R., Sigg, B., Horanyi, S. & Hudina, M. 2000 Local velocity measurements in a thermally-stratified sodium mixing layer using a permanent-magnet probe. *Expl Thermal Fluid Sci.* **20**, 115–136.

Knebel, J. U. & Krebs, L. 1994 Calibration of a miniature permanent magnet flow meter probe and its application to velocity measurements in liquid sodium. *Expl Thermal Fluid Sci.* **8**, 135–148.

Knebel, J. U., Krebs, L., Müller, U. & Axcell, B. P. 1998 Experimental investigation of a confined heated sodium jet in a co-flow. *J. Fluid Mech.* **368**, 51–79.

Kolmogorov, A. N. 1941 Local structure of turbulence in an incompressible fluid at very large Reynolds numbers. *Dokl. Akad. Nauk SSSR* **30**, 299–303.

Kraichnan, R. H. 1965 Inertial range spectrum in hydromagnetic turbulence. *Phys. Fluids* **8**, 1385–1387.

Larmor, J. L. 1919 How could a rotating body such as the sun become a magnet? *Report of the 87th Meeting of the British Association for the Advancement of Science, Bournemouth, Morray, London*, pp. 159–160.

Lowes, F. J. & Wilkinson, I. 1968 Geomagnetic dynamo: an improved laboratory model. *Nature* **219**, 717–718.

Moreau, R. 1990 *Magnetohydrodynamics*. Kluwer

Müller, U. & Stieglitz, R. 2000 Can the earth magnetic field be simulated in the laboratory?, *Naturwissenschaften* **87**, 381–390.

Müller, U. Stieglitz, R. & Horanyi, S. 2004 A two-scale hydromagnetic dynamo experiment. *J. Fluid Mech.* **498**, 31–71.


https://doi.org/10.1017/S0022112006008779 Published online by Cambridge University Press

Ponomarenko, Y. B. 1973 The theory of the hydromagnetic generator. *J. Appl. Mech. Tech. Phys.* **14**, 775–778.

Rädler, K. H. 1999 *From the Sun to the Great Attractor Guanajuato Lectures on Astrophysics.* Lecture Notes in Physics. Springer.

Rädler, K. H. & Cebers, A. (ed.) 2002 MHD Dynamo Experiments. Special issue of *Magnetohydrodynamics* **38**, 3–218.

Rädler, K. H., Rheinhard, M., Apstein, E. & Fuchs, H. 2002*a* On the mean-field theory of the Karlsruhe dynamo experiment: 1. Kinetic theory. *Magnetohydrodynamics* **38**, 41–71.

Rädler, K. H., Rheinhard, M., Apstein, E. & Fuchs, H. 2002*b* On the mean-field theory of the Karlsruhe dynamo experiment: 2. Back-reaction of the magnetic field on the fluid flow. *Magnetohydrodynamics* **38**, 73–94.

Ricou, R. & Vives, Ch. 1982 Local velocity and mass transfer measurements in molten metal using an incorporated magnet probe. *Intl J. Heat Mass Transfer* **25**, 1579–1588.

Rüdiger, G. & Hollerbach, R. 2004 *The Magnetic Universe.* Wiley-VCH.

Schlichting, H. 1958 *Grenzschicht-Theorie.* G. Braun, Karlsruhe.

Shercliff, J. A. 1965 *A Textbook of Magnetohydrodynamics.* Pergamon.

Stieglitz R. & Müller, U. 1996 *Geodynamo: Eine Versuchsanlage zum Nachweis des homogenen Dynamoeffects.* Wissenschaftlicher Bericht FZKA 5716.

Stieglitz, R. & Müller, U. 2001 Experimental demonstration of the homogeneous two-scale dynamo. *Phys. Fluids* **13**, 561–564.

Tilgner, A. 2002 Numerical simulation of the onset of dynamo action in an experimental two-scale dynamo. *Phys. Fluids* **14**, 4092–4094.

Weissenfluh, Th. 1985 Probes for local velocity and temperature measurements in liquid metal flow. *Intl J. Heat Mass Transfer* **28**, 1563–1574.

https://doi.org/10.1017/S0022112006008779 Published online by Cambridge University Press